Multiple Faults Isolation For Multi-Constellation GNSS Positioning through Incremental Expansion of Consistent Measurements

Penggao Yan, Yingjie Hu, Welson Wen, Li-Ta Hsu *Senior Member, IEEE*

***Abstract*— Fast and accurate fault detection and isolation for multiple faults is crucial for satellite navigation systems. However, conventional deletion-based greedy search methods suffer from swamping effects, i.e., wrongly excluding healthy measurements, which leads to degradation in positioning performance after executing the isolation. This study proposes an incrementally expanding algorithm to isolate multiple faulty measurements in the multi-constellation global navigation satellite system positioning. The proposed algorithm is designed to find the most consistent set by incrementally expanding the minimum basic set with fault-free assumption. In each iteration, the no-fault hypothesis testing is conducted on the ordered studentized and jackknife residuals, enabling the correction of the fault-free assumption made in constructing the minimum basic set. The isolation performance and its impacts on positioning accuracy are evaluated in a worldwide simulation. The proposed method shows a 26% reduction in the swamping event rate and a 75% reduction in the mean post-isolation positioning error, compared to the deletion-based greedy search method. Through Monte Carlo simulations, the stability of the proposed method regarding the number of faults and the fault magnitude is demonstrated. An application to the real-world dataset with artificially injected bias is also studied, showing a reduced post-isolation positioning error.**

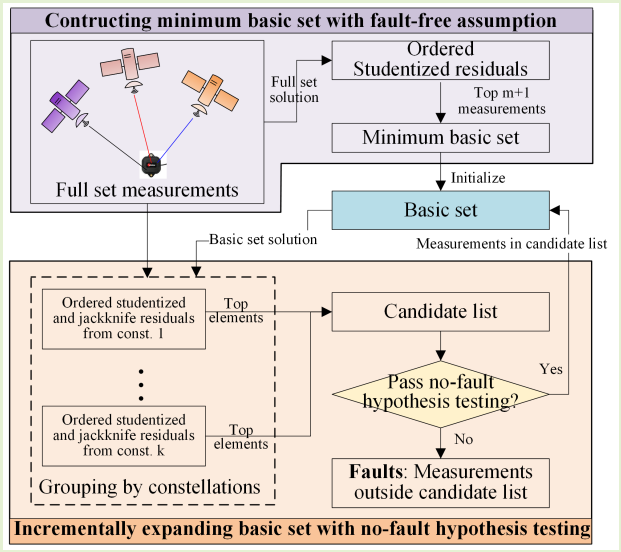

***Index Terms*— Multiple faults, fault detection and isolation, satellite navigation, jackknife, hypothesis testing, greedy search**

I. Introduction

FAST and accurate fault detection and isolation (FDI) is essential for satellite-based navigation systems in some safety-critical applications [1]–[5]. Fault detection is a technology to check the occurrence of faults in the system, while fault isolation aims to separate faulty measurements from healthy measurements [6], [7]. In this paper, we define faults as unmodelled measurement errors that substantially compromise the positioning solution, such as non-line-of-sight (NLOS) errors [4], [8], [9]. Those measurement errors that have relatively smaller impacts and are induced by environments are regarded as nominal measurement errors. Indeed, there is some intersection between the nominal measurement errors and the faults, which makes it difficult to distinguish the difference in a sole satellite-based positioning system. Therefore, the definition of faults and nominal measurement error emphasizes the impacts of measurements on the positioning solution.In satellite navigation research, the FDI technique can be roughly classified into two categories, including the snapshot approaches and sequential approaches. In snapshot approaches, measurements in a single epoch are used to develop test statistics, which can realize a fast detection of abrupt faults. In the sequential approaches, measurements used to calculate the test statistic are not limited to a single epoch. In addition, the sequential approaches usually involve the integration of different types of measurements, such as global navigation satellite system (GNSS) and inertial navigation system (INS) measurements [10], [11]. In this paper, we limit the scope to the snapshot approaches that use standalone GNSS measurements.

In the early stage of satellite navigation with limited satellites in operation, the snapshot FDI technique, such as the range comparison method [12], chi-squared test detector [13], parity space [14], [15], and the multiple hypothesis solution separation detector [16] in the conventional receiver autonomous integrity monitoring (RAIM) scheme [17], mainly focuses on the single fault case. However, with the growing

This work was supported by the RGC Collaborative Research Fund C5032-23G (Project: Heterogeneity-aware Collaborative Edge AI Acceleration).

Manuscript received xxx; revised xxx.

number of satellites and constellations, the probability of simultaneous faults becomes nonnegligible. For example, multiple Global Positioning System (GPS) satellites experienced high L1 single-frequency range errors of up to $16\,\mathrm{m}$ due to an erroneous ionospheric correction term between May 28 and June 2, 2002 [18]. Moreover, in urban applications, multiple pseudorange measurement faults frequently occur due to the presence of multipath and non-line-of-sight (NLOS) signals. These highlight the need for FDI techniques in handling multiple faults [19]. In fact, researchers have already proposed an optimal FDI algorithm under some assumptions [20]. This algorithm involves evaluating the consistency of all sets of measurements and selecting the best set with the highest level of consistency. The implementation of this algorithm in the navigation community can refer to the multiple-hypothesis solution separation for multiple faults integrity monitoring [21]. Nevertheless, this algorithm relies on combinatorial search, which becomes computationally intractable as the number of measurements grows [20]–[22]. For example, $2^{20} \sim 10^6$ sets have to be examined when considering all 10 or more measurement combinations with 21 measurements in the three-constellation setting. A detailed discussion of its computation load in satellite navigation applications is given in [21]. Therefore, it is essential to develop methods that can achieve combinatorial search performance at a lower computational cost.

To overcome the exponentially increasing computation time of exhaustive search algorithm, deletion-based greedy search method have been proposed [21], [23]–[25]. Mathematically speaking, the deletion-based greedy search method consistently removes sets of measurements to reduce the properly chosen statistic. For example, Blanch et al. [21] propose the greedy search method by removing the measurement with the largest normalized residual in an iterative process. The algorithm stops when the weighted sum of square error (WSSE) is below the consistency threshold. Hsu et al. [26] propose the iterative consistency check method by excluding the measurement that results in the largest reduction in the WSSE. Knowles and Gao [22] propose the greedy Euclidean distance matrix (EDM) algorithm, which iteratively eliminates the largest average absolute value of the fourth and fifth eigenvalues. The algorithm stops when the fault detection test statistic falls below a given threshold. Although these deletion-based methods produce competitive performances compared to the exhaustive search method, they are unavoidably affected by the swamping effect [27], i.e., healthy measurements are incorrectly identified as faults, and tests based on them lose their powers substantially in the presence of multiple outliers [27], [28]. The swamping effect could be extraordinarily dangerous because the exclusion operation reduces the redundancy of healthy measurements, subsequently increasing the risk of large positioning deviation.

In this study, an expanding-based greedy search method is proposed for fast and accurate FDI in pseudorange-based positioning systems. Unlike the mainstream deletion-based greedy search methods, the proposed method incrementally expands the measurement set until the faults are detected. Due to its expanding nature, the proposed method is more resistant to the swamping effect than the deletion approach. This idea is not new, and some practices on the outlier-detection for linear regression problems can be found in the statistic literature [29], [30]. However, when it comes to the multiple fault isolation problem in multi-constellation GNSS positioning systems, some practical considerations need to be taken into account. The unique characteristics of such systems, including the heterogeneity of measurements from different constellations, introduce new challenges that cannot be adequately addressed by the existing practices in the statistical literature. Moreover, these studies [29], [30] mainly focus on the detection performance and ignore the isolation effects on the estimation results, e.g., the positioning error, which is extremely important in positioning applications. Therefore, this study aims to extend the incrementally expanding idea to detect and isolate multiple fault measurements in multi-constellation GNSS positioning systems, and to comprehensively analyze its isolation performance and its impacts on positioning accuracy. Specifically, the proposed algorithm starts with constructing a minimum basic set, which has the minimum studentized residual computed based on full-set measurements. A grouping-based approach considering the heterogeneity of different constellations is proposed to sort the measurements according to their studentized and jackknife residual. Then the basic set is expanded with no-fault hypothesis testing by examining the cut-off points of the ordered residuals. Since the no-fault hypothesis testing is a multiple-testing problem, the Bonferroni correction [31] is further applied to correct the threshold in testing. The expanding process is repeated until a fault is detected.

The proposed method is evaluated in a simulated experiment to isolate multiple pseudorange faults for a set of users distributed over the world during one day. In the worldwide simulation experiments with nine injected faults and the magnitude uniformly distributed in $[-50\,\mathrm{m}, -25\,\mathrm{m}] \cup [25\,\mathrm{m}, 50\,\mathrm{m}]$, the proposed method exhibits a more than $26\,\%$ reduction in the mean swamping event rate, compared to the deletion-based greedy search method [21]. In addition, the mean positioning error of the proposed method is around $75\,\%$ less than the deletion-based greedy search method. Moreover, in the Monte-Carlo simulation, the proposed method shows a more stable performance than the greedy search method regarding the number of faults and fault magnitude. The mean computation time on the three-constellation setting is less than $30\,\mathrm{ms}$ when the number of faults ranges from 2 to 15, which is comparable to the greedy search method. An application to the real-world dataset with artificially injected bias is also studied, showing a similar result to the simulation experiments. The contributions of this study are two folds:

1) Propose an accurate and fast multiple fault isolation algorithm for multi-constellation GNSS positioning systems. The expanding nature of the proposed method can effectively prevent performance degradation by reducing the events of wrong exclusion of healthy measurements;
2) Conduct extensive simulations and a real-world experiment to demonstrate the improved isolation performance and stability of the proposed method compared to the

deletion-based greedy search method.

II. Backgrounds on Studentized Residuals for Pseudorange-based Positioning System

This section briefly introduces the construction of studentized and jackknife residuals for a pseudorange-based positioning system, providing the theoretical basis for the development of the proposed incrementally expanding fault isolation algorithm in Section III.

A. Linearization of Pseudorange-based Positioning Systems

A generalized linear system for pseudorange-based positioning can be written as

$$\mathbf{y} = \mathbf{H}\Delta\mathbf{x} + \boldsymbol{\varepsilon}\,, \tag{1}$$

where

$$\mathbf{y} = \begin{bmatrix} f\left(\rho_1, \mathbf{x}_0\right) \\ \vdots \\ f\left(\rho_n, \mathbf{x}_0\right) \end{bmatrix}, \mathbf{H} = \begin{bmatrix} \mathbf{h}\left(\{\mathbf{p}^{1,j}\}, \mathbf{x}_0\right) \\ \vdots \\ \mathbf{h}\left(\{\mathbf{p}^{n,j}\}, \mathbf{x}_0\right) \end{bmatrix}, \boldsymbol{\varepsilon} = \begin{bmatrix} \varepsilon_1 \\ \vdots \\ \varepsilon_n \end{bmatrix}, \quad \Delta\mathbf{x} = \mathbf{x} - \mathbf{x}_0\,, \tag{2}$$

$f\left(\rho_i, \mathbf{x}_0\right)$ is a function of the ith measurement ρ_i (note that ρ_i refers to a generalized measurement, not limited to the pseudorange measurement) and the linearized point $\mathbf{x}_0$; $\mathbf{h}\left(\{\mathbf{p}^{i,j}\}, \mathbf{x}_0\right)$ is a vector function of the collection of satellite positions $\{\mathbf{p}^{i,j}\}$ related to the ith measurement and $\mathbf{x}_0$; $\mathbf{x}$ is the receiver positioning state (an $m \times 1$ vector); and ε_i is the ith measurement error and is assumed to have a zero-mean Gaussian distribution. Furthermore, it is assumed that $\boldsymbol{\varepsilon} \sim \mathcal{N}(0, \delta^2\boldsymbol{\Sigma})$, where $\boldsymbol{\Sigma}$ is a diagonal matrix and δ is a constant.

B. Studentized and Jackknife Residuals

Divide the full n measurements into two disjoint sets, i.e., the basic set $\mathcal{B}$ (containing s elements) and the non-basic set $\mathcal{O}$ (containing $n - s$ elements). In this paper, it is assumed that the basic set is free of fault. Section III gives the details of determining the basic set. Using measurements in the basic set, the estimated receiver positioning state $\hat{\mathbf{x}}_\mathcal{B}$ can be obtained by implementing the weighted least square (WLS) method (in an iterative approach) as follows:

$$\Delta\hat{\mathbf{x}}_\mathcal{B} = \mathbf{G}_\mathcal{B}\mathbf{y}_\mathcal{B} \tag{3a}$$

$$\hat{\mathbf{x}}_\mathcal{B} = \mathbf{x}_0 + \Delta\hat{\mathbf{x}}_\mathcal{B}\,, \tag{3b}$$

where

$$\mathbf{G}_\mathcal{B} = \left(\mathbf{H}_\mathcal{B}^T\mathbf{W}_\mathcal{B}\mathbf{H}_\mathcal{B}\right)^{-1}\mathbf{H}_\mathcal{B}^T\mathbf{W}_\mathcal{B} \tag{4}$$

is the projection matrix, and $\mathbf{W}_\mathcal{B} = \boldsymbol{\Sigma}_\mathcal{B}^{-1}$ is the weighting matrix. The subscript $\mathcal{B}$ in (3) indicates that the corresponding variable is defined with respect to the set $\mathcal{B}$.

The studentized residual [32] in WLS can be derived as (a detailed derivation is given in Appendix I):

$$r_i = \frac{\sqrt{w_{\mathcal{I}_\mathcal{B}(i)}}y_i - \sqrt{w_{\mathcal{I}_\mathcal{B}(i)}}\mathbf{h}_{\mathcal{I}_\mathcal{B}(i)}\Delta\hat{\mathbf{x}}_\mathcal{B}}{\hat{\delta}_\mathcal{B}\sqrt{1 - g_{\mathcal{I}_\mathcal{B}(i)}}}, y_i \in \mathcal{B}\,, \tag{5}$$

where y_i is the ith element in the full set and belongs to $\mathcal{B}$, $\mathcal{I}_\mathcal{B}(\cdot)$ is a function to identify the index of y_i in $\mathcal{B}$, $w_{\mathcal{I}_\mathcal{B}(i)}$ is the $\mathcal{I}_\mathcal{B}(i)$th element on the diagonal of $\mathbf{W}_\mathcal{B}$, $\mathbf{h}_{\mathcal{I}_\mathcal{B}(i)}$ is the $\mathcal{I}_\mathcal{B}(i)$th row of $\mathbf{H}_\mathcal{B}$, $g_{\mathcal{I}_\mathcal{B}(i)}$ is the $\mathcal{I}_\mathcal{B}(i)$th element on the diagonal of $\mathbf{G}_\mathcal{B}$, and

$$\hat{\delta}_\mathcal{B} = \sqrt{\frac{\left(\mathbf{y}_\mathcal{B} - \mathbf{H}_\mathcal{B}\Delta\hat{\mathbf{x}}_\mathcal{B}\right)^T\mathbf{W}_\mathcal{B}\left(\mathbf{y}_\mathcal{B} - \mathbf{H}_\mathcal{B}\Delta\hat{\mathbf{x}}_\mathcal{B}\right)}{s - m}} \tag{6}$$

is the estimation of δ using data in the basic set $\mathcal{B}$. With the Gaussian assumption $\boldsymbol{\varepsilon} \sim \mathcal{N}(0, \delta^2\boldsymbol{\Sigma})$ in Section II-A, the studentized residual r_i has a relationship to beta-distributed variables as follows [32] :

$$\frac{r_i^2}{s - m} \sim \beta\left(\frac{1}{2}, \frac{s - m - 1}{2}\right). \tag{7}$$

The jackknife residual [33], [34] can be derived as (a detailed derivation is given in Appendix I)

$$t_i = \frac{\sqrt{w_i}y_i - \sqrt{w_i}\mathbf{h}_i\Delta\hat{\mathbf{x}}_\mathcal{B}}{\hat{\delta}_\mathcal{B}\sqrt{1 + w_i\mathbf{h}_i\left(\mathbf{H}_\mathcal{B}^T\mathbf{W}_\mathcal{B}\mathbf{H}_\mathcal{B}\right)^{-1}\mathbf{h}_i^T}}, y_i \in \mathcal{O}\,, \tag{8}$$

where w_i is the ith element on the diagonal of $\mathbf{W}$, and $\mathbf{h}_i$ is re-constructed based on the linearized point $\mathbf{x}_0$ as follows:

$$\mathbf{h}_i = \mathbf{h}\left(\{\mathbf{p}^{i,j}\}, \mathbf{x}_0\right), y_i \in \mathcal{O}\,. \tag{9}$$

The definition of $\mathbf{h}(\cdot)$ can be found in (2). With the Gaussian assumption $\boldsymbol{\varepsilon} \sim \mathcal{N}(0, \delta^2\boldsymbol{\Sigma})$ in Section II-A, the jackknife residual has a t-distribution [34]:

$$t_i \sim t(s - m)\,. \tag{10}$$

Both the studentized residual and the jackknife residual are a dimensionless quantity that measures the difference between the predicted and observed values of each y_i. The proposed incrementally expanding isolation algorithm will utilize these residuals to identify potential faults.

III. Incrementally Expanding Methods for Multiple Faults Isolation

The proposed algorithm aims to find the most consistent set in an incrementally expanding approach. The proposed algorithm mainly consists of two steps, including the minimum basic set construction and the incrementally expanding with no-fault hypothesis testing.

A. Constructing the minimum basic set

The proposed algorithm starts with constructing a minimum basic set $\mathcal{B}$ with $m+1$ measurements, which has the minimum studentized residual computed based on the full-set measurements. Algorithm 1 shows the pseudocode of the construction process. First, the full-set solution $\hat{\mathbf{x}}$ is calculated using all n measurements (utilizing WLS in an iterative approach),

$$\Delta\hat{\mathbf{x}} = \left(\mathbf{H}^T\mathbf{W}\mathbf{H}\right)^{-1}\mathbf{H}^T\mathbf{W}\mathbf{y} \tag{11a}$$

$$\hat{\mathbf{x}} = \mathbf{x}_0 + \Delta\hat{\mathbf{x}}\,, \tag{11b}$$

where $\mathbf{W} = \boldsymbol{\Sigma}^{-1}$ is the weighting matrix. For each measurement, the corresponding studentized residual is calculated according to (5) (lines 1–4). In this calculation, the basic set $\mathcal{B}$

is the full set. Then the n studentized residuals are ordered in ascending order, and the first $m+1$ measurements are chosen to construct the minimum basic set (lines 5–6).

As can be seen, the minimum basic set is constructed solely based on the ranking of studentized residuals. For simple linear regression problems, as the one in [29], the minimum basic set can be directly used to calculate the jackknife residuals of measurements out of the minimum basic set. However, for the multi-constellation GNSS system, the minimum basic set may only contain measurements from one or two constellations, making it impossible to calculate the jackknife residual of measurements from constellations that are not included in the minimum basic set. This is because the calculation of the jackknife residual relies on the geometry matrix and the solution obtained based on the minimum basic set, as shown in (8). For example, assuming that the minimum basic set contains measurements from the GPS and GALILEO constellations, the solution obtained based on the minimum basic set is a five-dimensional vector, consisting of the three-dimensional positioning vector, the receiver clock bias from the GPS constellation, and the receiver clock bias from the GALILEO constellation. When calculating the jackknife residual of a measurement from the GLONASS constellation, the term $\Delta\hat{\mathbf{x}}_{\mathcal{B}}$ in (8) involves the estimation of the three-dimensional position and the receiver clock bias from the GLONASS constellation. Unfortunately, the estimation of the receiver clock bias from the GLONASS constellation is unknown; therefore, it is impossible to calculate the jackknife residual of measurement from the GLONASS constellation when the minimum basic set does not contain measurements from the GLONASS constellation.

To tackle this issue, the minimum basic set is augmented to ensure that at least one measurement from each constellation is included in the augmented minimum basic set. Specifically, the measurements associated with the ordered studentized residuals are sequentially examined (line 9). The first measurement from the constellation that is not included in the minimum basic set is added to the minimum basic set (line 10). This process is repeated until the minimum basic set contains at least one measurement from each constellation. The augmentation will add at most $k-1$ measurements into the original minimum basic set, where k is the number of constellations of the GNSS system. For example, at most two measurements will be added to the minimum basic set in the three-constellation GNSS system. The remaining measurements formalize the non-Basic set $\mathcal{O}$.

B. Incrementally expanding basic set with no-fault hypothesis testing

In the second step, the minimum basic set is incrementally expanded by the remaining measurements with no-fault hypothesis testing until faults are detected. The minimum basic set is expected to be free of faulty measurements, which, however, is a strong assumption. Therefore, a remedial philosophy is also integrated into the subsequent procedure in case the assumption is violated. Algorithm 2 shows the pseudocode of the expanding process.

Algorithm 1 Minimum Basic Set Construction

Input:
Measurements: $\Xi = \{y_1, y_2, \cdots, y_n\}$
Size of the positioning state: m
Output:
The minimum basic set: $\mathcal{B}$
// Constructing the minimum basic set
1: **for each** $y_i \in \Xi$ **do**
2: Compute the studentized residual t_i with Ξ ▷ Eq. (5)
3: $\mathcal{T} \leftarrow |t_i|$
4: **end for**
5: Order $\mathcal{T}$ in ascending order
6: $\mathcal{B} \leftarrow$ Elements in Ξ that corresponds to the top $m+1$ elements in the ordered $\mathcal{T}$
// Augmenting the minimum basic set
7: $\Gamma =$ {Constellations not included in $\mathcal{B}$}
8: **for each** $\gamma \in \Gamma$ **do**
9: $|t_i| \leftarrow$ The smallest element in $\mathcal{T}$ from const. γ
10: $\mathcal{B} \leftarrow$ The measurement corresponding to $|t_i|$
11: **end for**
12: Return $\mathcal{B}$

1) The naive approach to expand the basic set: A naive approach to expand the basic set is to arrange the measurements in ascending order according to t_i ($y_i \in \mathcal{B}$ for studentized residual, while $y_i \in \mathcal{O}$ for jackknife residual) and then select the first $s+1$ ordered measurements as the new basic set. Here, s is the size of the current basic set. This approach is well-adopted in simple linear regression problems [29], [35]. However, in the multi-constellation positioning system, such the method ignores the fact that jackknife (or studentized) residuals associated with different constellations are heterogeneous, and hence not comparable.

The heterogeneity is primarily attributed to the usage of the estimated receiver clock bias in the calculation of jackknife and studentized residuals. Taking the jackknife residual in (8) for example, the term $\mathbf{h}_i\Delta\hat{\mathbf{x}}_{\mathcal{B}}$ in the numerator can be rewritten as

$$\mathbf{h}_i\Delta\hat{\mathbf{x}}_{\mathcal{B}} = \mathbf{e}_i[\hat{x}_{\mathcal{B}}, \hat{y}_{\mathcal{B}}, \hat{z}_{\mathcal{B}}]^T + \hat{\delta}_{\mathcal{B}}^{\mathbb{I}(y_i)} \tag{12}$$

where $\mathbf{e}_i$ is the 1×3 line-of-sight vector of the measurement y_i, $[\hat{x}_{\mathcal{B}}, \hat{y}_{\mathcal{B}}, \hat{z}_{\mathcal{B}}]$ is the estimated three-dimensional position vector based on the basic set, and $\hat{\delta}_{\mathcal{B}}^{\mathbb{I}(y_i)}$ is the estimated receiver clock bias of the constellation that y_i comes from. For two measurements from different constellations, their jackknife residuals use different estimations of the receiver clock bias, each of which is calculated by the measurements from the corresponding constellation in the basic set. Therefore, only the jackknife residuals from the same constellation are comparable as they use the same position and receiver clock bias estimations. Similarly, the studentized residual also has heterogeneity in the usage of receiver clock bias estimations.

2) The grouping-based approach to expand the basic set: To tackle this heterogeneity issue, a grouping-based approach is proposed to expand the basic set. First, the full set measurements Ξ are grouped according to their constellations (lines 6–8). Within each group, t_i ($y_i \in \mathcal{B}$ for studentized residual,

Algorithm 2 Incrementally Expanding Algorithm for Multiple Faults Isolation

Input:
Measurements: $\Xi = \{y_1, y_2, \cdots, y_n\}$
Size of the positioning state: m
Number of measurements: n
Upper limit of the type I error for an individual test: α
Output:
Set of faulty measurements: $\mathcal{F}$
// Construction of the minimum basic set
1: The minimum basic set: $\mathcal{B} \leftarrow$ Algorithm 1 with Ξ, m
2: $s \leftarrow$ Size of $\mathcal{B}$
3: **while** $s + 1 < n$ **do**
// Grouping-based expanding
4: Construct the non-basic set: $\mathcal{O} = \Xi \setminus \mathcal{B}$
5: $\mathcal{S} = \emptyset$ ▷ Initialize the set for hypothesis testing
6: $\Gamma =$ {Constellations included in $\mathcal{B}$}
7: **for each** $\gamma \in \Gamma$ **do**
8: $\Xi_\gamma \leftarrow$ Measurements from constellation γ in Ξ
9: $\mathcal{B}_\gamma \leftarrow$ Measurements from constellation γ in $\mathcal{B}$
10: **for each** $y_i \in \Xi_\gamma$ **do**
11: **if** $y_i \in \mathcal{B}$ **then**
12: $t_i \leftarrow$ Studentized residual on $\mathcal{B}$ ▷ Eq. (5)
13: **else**
14: $t_i \leftarrow$ Jackknife residual on $\mathcal{B}$ ▷ Eq. (8)
15: **end if**
16: $\mathcal{T}_\gamma \leftarrow |t_i|$
17: **end for**
18: Order $\mathcal{T}_\gamma$ in ascending order
19: $\mathcal{S} \leftarrow$ Elements in Ξ_γ corresponding to the top $|\mathcal{B}_\gamma|$ elements in the ordered $\mathcal{T}_\gamma$
20: **end for**
21: $\mathcal{S} \leftarrow$ The element in $\Xi \setminus \mathcal{S}$ corresponding to the smallest $|t_i|$
// No-fault hypothesis testing
22: **for each** $y_i \in \mathcal{S}$ **do**
23: **if** $y_i \in \{y_i | y_i \in \mathcal{S}, y_i \in \mathcal{B}\}$ and (13a) is true **then**
24: **go to** line 33
25: **end if**
26: **if** $y_i \in \{y_i | y_i \in \mathcal{S}, y_i \notin \mathcal{B}\}$ and (13b) is true **then**
27: **go to** line 33
28: **end if**
29: **end for**
30: $\mathcal{B} = \mathcal{S}$ ▷ Update the basic set
31: $s \leftarrow$ Size of $\mathcal{B}$
32: **end while**
33: Return $\mathcal{F} = \{y_i | y_i \notin \mathcal{S}\}$

while $y_i \in \mathcal{O}$ for jackknife residual) is calculated for each measurement (lines 10–17). Taking the group Ξ_γ for example, where all measurements come from the constellation γ, the measurements in that group are arranged in ascending order according to $|t_i|$, and the first $|\mathcal{B}_\gamma|$ measurements are added to the no-fault candidate set $\mathcal{S}$ for hypothesis testing in Section III-B.3 (lines 18–19). Here, $\mathcal{B}_\gamma$ is the set of measurements from constellation γ in the current basic set $\mathcal{B}$, and $|\mathcal{B}_\gamma|$ is its size. Finally, in the remaining measurements $\Xi \setminus \mathcal{S}$, the one has the smallest t_i are selected to expand the candidate set $\mathcal{S}$ (line 21).

The grouping-based expanding approach ensures that the no-fault candidate set $\mathcal{S}$ contains at least the same number of measurements as the current basic set $\mathcal{B}$ for each constellation, preventing the number of constellations from decreasing. The maintenance of the number of constellations is essential, as will be shown in the subsequent procedure. Moreover, as the set $\mathcal{S}$ is constructed by measurements that have the smallest $|t_i|$'s in each group (lines 7–21), $|t_i|$'s of non-basic set elements could be smaller than those of the basic set elements. Therefore, some elements of the basic set may be eliminated during this process. Recall that the free-of-fault assumption is made in constructing the minimum basic set in Section III-A. This assumption is gradually repaired by this re-ordering mechanism.

3) No-fault hypothesis testing: The no-fault candidate set $\mathcal{S}$ is employed for the following no-fault hypothesis testing:

$$H_0\text{: No faults in } \mathcal{S}$$
$$H_1\text{: At least one fault exists in } \mathcal{S}\,.$$

The above testing aims to examine whether $\mathcal{S}$ is consistent with the current basic set $\mathcal{B}$. If H_0 is not rejected, the basic set will be augmented by the set $\mathcal{S}$, which implies the expanding nature of the algorithm.

The set $\mathcal{S}$ contains both basic and non-basic set elements, and therefore they should be examined separately. Specifically, the measurements in $\mathcal{S}$ are divided into two parts, i.e., $\mathcal{S}_\mathcal{B} = \{y_i | y_i \in \mathcal{S}, y_i \in \mathcal{B}\}$ and $\mathcal{S}_\mathcal{O} = \{y_i | y_i \in \mathcal{S}, y_i \notin \mathcal{B}\}$. The following statements are examined (lines 21–28),

$$\frac{\max |t_i|^2}{s-m} \geq \beta^{-1}_{\frac{1}{2}, \frac{s-m-1}{2}}\left(1 - \frac{\alpha}{s+1}\right), y_i \in \mathcal{S}_\mathcal{B} \tag{13a}$$
$$\max |t_i| \geq t^{-1}_{s-m}\left(1 - \frac{\alpha}{2(s+1)}\right), y_i \in \mathcal{S}_\mathcal{O}\,, \tag{13b}$$

where $s+1$ is the size of $\mathcal{S}$, and α is the upper limit of the type I error for an individual test. The above testing is a multiple testing problem, and therefore the Bonferroni correction [31] is applied when setting the testing threshold. The type I error for an individual test ranges from $\frac{\alpha}{s+1}$ to α due to the Bonferroni correction [31]. By examining the above statements, we have the following two situations:

1) If at least one of the statements in (13) is examined to be true, H_0 is reject (lines 23 –28). Then measurements $y_i \notin \mathcal{S}$ are claimed to be outliers, and the algorithm stops;
2) Otherwise, $\mathcal{S}$ is regarded as the new basic set (line 30), and we repeat the process in Section III-B until $n = s + 1$.

Note that in the second situation, $\mathcal{S}$ is regarded as the new basic set. Since the grouping-based expanding approach in Section III-B.2 maintains the number of constellations in $\mathcal{S}$, it is possible to calculate the jackknife residual of any measurement based on the new basic set (i.e, $\mathcal{S}$) in the next iteration (line 14).

IV. Isolation and Positioning Performance with Worldwide Simulations

A. Experiment Setting and Evaluation Metrics

The proposed method is employed to isolate multiple faults for a set of users distributed over the world during one day. The MATLAB algorithm availability simulation tool (MAAST) developed at Stanford University [36], is utilized to simulate the dual frequency pseudorange measurements, satellite positions, and user locations. Specifically, we investigate the case of three constellations (the 24-satellite GPS constellation, the 30-satellite Galileo constellation, and the 23-satellite GLONASS constellation) and four constellations (the aforementioned three constellations and a 27-satellite BEIDOU constellation) in simulating satellite positions. The users are placed on a grid every 10 degrees longitude and latitude (which gives 648 locations). For each location, the geometries are simulated every 5 minutes (which gives 288 time steps). The measurement error is simulated as the zero-mean Gaussian distribution with the same configuration in [37]. For each time and user location, a given number of measurements are randomly chosen for additional bias injection. Each bias is generated from a uniform distribution. The experiment setting is summarized in Table I. The following will focus on the results of the three-constellation experiment. Additional results of the four-constellation experiments can be found in Appendix III.

TABLE I: Parameters of worldwide simulations with three constellations

Constellations	Number of faults	Fault magnitude	Alpha
GPS, Galileo, GLONASS	9	$[-50\,\mathrm{m}, -25\,\mathrm{m}] \cup [25\,\mathrm{m}, 50\,\mathrm{m}]$	0.05

In order to evaluate the performance of the fault isolation algorithm, three kinds of events are defined by examining the isolation results, including the exactly correct detecting, swamping, and masking events, as follows:

(1) Exactly correct detecting event

All faulty measurements are correctly separated from nominal measurements. The rate of exactly correct detecting events can be defined as

$$P_1 = \frac{\text{Number of exactly correct detecting events}}{\text{Total epochs}}. \quad (14)$$

(2) Swamping event

At least one nominal measurement is incorrectly identified as a fault. The rate of swamping events can be defined as

$$P_2 = \frac{\text{Number of swamping events}}{\text{Total epochs}}. \quad (15)$$

(3) Masking event

None of the faulty measurements are identified. The rate of masking events can be defined as

$$P_3 = \frac{\text{Number of masking events}}{\text{Total epochs}}. \quad (16)$$

For each user location, P_1, P_2, and P_3 are calculated. A good detector is expected to have a high value of P_1 and a low values of P_2 and P_3. In addition, positioning accuracy is also an important issue regarding the context of satellite positioning. Therefore, the positioning error after the fault isolation process, i.e., the post-isolation positioning error, is calculated. A good detector for satellite positioning systems shall produce small post-isolation positioning errors.

B. Fault Isolation Performance Comparison

The proposed method is compared with the deletion-based greedy search algorithm [21]. At each step, the greedy search algorithm removes the measurement with the largest normalized residual. The algorithm stops when the weighted sum of square error is below the consistency threshold. A detailed introduction is given in Appendix II.

Table II summarizes the rate of the three kinds of events. Both methods have similar performance regarding the exact correct detecting event rate. Surprisingly, the deletion-based greedy search method has a significantly low masking event rate, which means that at least one faulty measurement can be identified by this method. However, the proposed method cannot guarantee this property because it is designed to find the largest consistency set. Nevertheless, this design philosophy actually benefits the positioning system in terms of positioning accuracy, which will be seen in Section IV-C. Actually, this benefit is reflected by its low swamping event rate, as shown in Tables II. The mean swamping event rate of the proposed method is only $8.78\,\%$, which is $26\,\%$ less than that observed in the deletion-based greedy search method. Notably, the maximum swamping event rate of the deletion-based greedy search method is around $58\,\%$, indicating that healthy measurements are frequently excluded. This could be very dangerous because the exclusion operation reduces the redundancy of healthy measurements, subsequently increasing the risk of large positioning deviation.

TABLE II: Isolation performance in the three-constellation experiment

	Incrementally expanding			Deletion-based greedy search		
Event	Exact	Swamping	Masking	Exact	Swamping	Masking
Max	**92.71** %	**14.24** %	20.14 %	87.85 %	57.99 %	**0** %
Mean	**80.22** %	**8.78** %	8.00 %	64.73 %	35.24 %	**0** %
Min	**61.11** %	**4.86** %	0.69 %	42.01 %	12.15 %	**0** %

C. Post-isolation Positioning Performance Comparison

To understand the effects of swamping events, we plot the map of post-isolation positioning error for both methods, as shown in Fig. 1. The value plotted is the 99.5 percentile of all the post-isolation positioning error values computed at a given location over the course of a day. In most user locations, the 99.5 percentile post-isolation positioning error of the deletion-based greedy search method is larger than $80\,\mathrm{m}$, as shown in Fig. 1b. Moreover, in a considerable number of user locations, this value even surpasses $100\,\mathrm{m}$. However, the 99.5 percentile post-isolation positioning error of the proposed method is less than $60\,\mathrm{m}$ at most locations, as shown in Fig. 1a. Finally,

it is interesting to find that the post-isolation positioning error of both methods in the high-latitude region is much smaller than that in the low-latitude region. The main reason is that there are more visible satellites in the high-latitude region [38], which provides more measurement redundancy. Since both the deletion-based and the expanding-based greedy-search FDI methods are designed to find the most consistent subset of measurements, an enlarged measurement redundancy can improve the detection and isolation performance given a fixed number of faults.

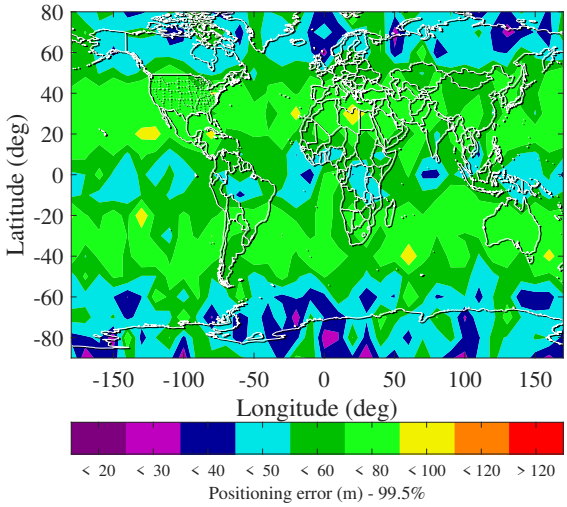

(a)

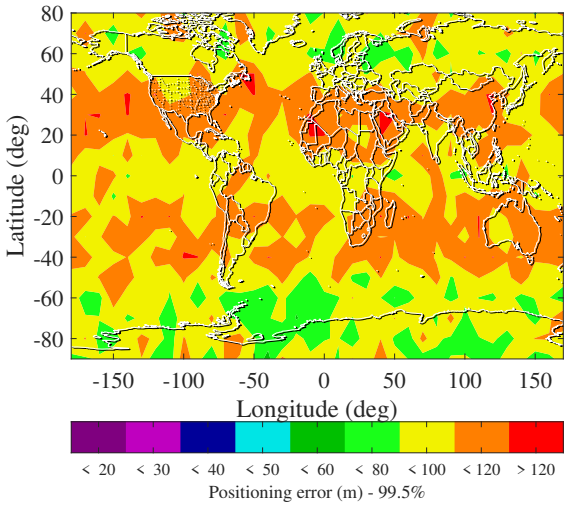

(b)

Fig. 1: 99.5 percentile of the post-isolation positioning error over the course of the day yielded by (a) the incrementally expanding algorithm and (b) the deletion-based greedy search algorithm in the worldwide simulation experiment with three constellations.

The statistics of the post-isolation positioning error of all location-time combinations are summarized in Table III. Notably, the maximum post-isolation positioning error of the deletion-based greedy search method is 7.62×10^{13} m. On the contrary, the maximum post-isolation positioning error of the proposed method retains a reasonable value of $181.58\,\mathrm{m}$. Expect the maximum value, the mean post-isolation positioning error is also an important metric to evaluate the positioning performance of fault isolation algorithms. However, the mean post-isolation positioning error of the deletion-based greedy search method can be affected by samples that have excessively large post-isolation positioning errors, making it less representative to describe the average positioning performance of the deletion-based greedy search method. Therefore, samples that have positioning errors larger than $1.000\,\mathrm{m}$ are manually excluded before calculating the mean post-isolation positioning error of the deletion-based greedy search method. This process excludes 12 samples and the resulting mean post-positioning error of the deletion-based greedy search method is $9.15\,\mathrm{m}$. Nevertheless, the proposed method yields a significantly smaller mean post-isolation positioning error, achieving a $75\,\%$ reduction. This phenomenon is actually reflected by the $99.5\,\%$ post-isolation positioning error map in Fig. 1.

TABLE III: Statistics of the post-isolation positioning error for all location-time combinations in the three-constellation experiment

Incrementally expanding			Deletion-based greedy search		
Max	Mean	Min	Max	Mean	Min
181.58 m	**2.28** m	0.01 m	7.62×10^{13} m	9.15 m[1]	0.01 m

[1] The mean value is calculated without samples whose positioning error is larger than 1.000 m.

V. Stability and Efficiency Analysis with Monte Carlo Simulation

This section investigates the stability and efficiency of the proposed incrementally expanding algorithm by conducting the Monte Carlo simulation. In the stability analysis, we investigate the impacts of the number of faults and fault magnitude on the isolation and post-isolation positioning performance of the proposed method and compare it with the deletion-based greedy search algorithm. In the efficiency analysis, we calculate the computation time of the proposed method against the number of faults.

A. Impacts of the Number of Faults

This section investigates the impacts of the number of faults on the isolation and post-isolation positioning performance of the proposed method. The Monte Carlo simulation is conducted by implementing the proposed method against different numbers of faults. Specifically, the satellite geometry that contains the largest number of satellites in the worldwide simulation experiment is adopted, as shown in Fig. 2. Then N satellites (measurements) are randomly selected for additional bias injection, where each bias is generated from a uniform distribution in the interval $[-50\,\mathrm{m}, -25\,\mathrm{m}] \cup [25\,\mathrm{m}, 50\,\mathrm{m}]$. We study the cases of $N = \{2, 3, 4, 5, 6, 7, 8, 9, 10, 11, 12, 13, 14, 15\}$, and for each case of N, we conduct 10,000 simulations. The simulation parameters are listed in the "case A" row in Table IV.

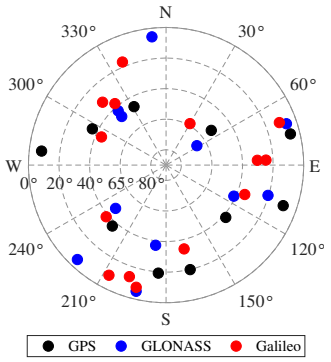

Fig. 2: Sky plots of the satellite geometry that contains the largest number of satellites in the worldwide simulation.

TABLE IV: Parameters of Monte Carlo simulations

Cases	Satellite geometry	Number of faults	Fault magnitude
A	Fig. 2	N[1]	$[-50\,\text{m}, -25\,\text{m}] \cup [25\,\text{m}, 50\,\text{m}]$
B	Fig. 2	9	$[-M^2\ \text{m}, -\frac{M}{2}\ \text{m}] \cup [\frac{M}{2}\ \text{m}, M\ \text{m}]$

[1] $N = \{2, 3, 4, 5, 6, 7, 8, 9, 10, 11, 12, 13, 14, 15\}$.
[2] $M = \{5, 10, 20, 30, 40, 50, 65, 80, 100\}$.

Fig. 3 shows the three event rates and the post-isolation positioning error of the proposed algorithm against the number of faults. The deletion-based greedy search algorithm is also implemented in the same procedure, and its results are summarized in Fig. 3 for comparison. With the increase in the number of faults, the exactly correct detecting event rate of both methods shows a decreasing trend. Both methods have a nearly constant swamping event rate when $N < 9$. However, when N exceeds 9, the swamping event rate of the proposed method experiences a significant decrease. This phenomenon can be explained by the expanding nature of the proposed method. When the number of faults is quite large, there is a high probability for a faulty measurement to be absorbed into the basic set during the expanding process. Moreover, since the proposed method is designed to find the largest consistency set, the expanding process tends to absorb more nominal measurements to balance the impacts of fault measurements on the inner-set consistency. Therefore, the proposed method has less chance to exclude nominal measurements, thereby achieving a smaller swamping event rate. Since the proposed method tends to retain some faulty measurements instead of excluding them when the number of faults is significant, the positioning system can use more measurements for positioning solution, which actually prevents the system from geometry collapse. As illustrated in Section III, the proposed method is designed to find the largest consistency set. This design philosophy actually avoids the situation of geometry collapse, where the set shows the most inconsistency (accompanied by excessive positioning error). However, the deletion-based method always excludes the suspected faulty measurement with respect to the current measurement set, even if the current measurement set is dominated by faulty measurements. Therefore, the deletion-based greedy search method would experience performance degradation when the number of faults increases, as indicated by Fig. 3(b) and Fig. 3(d). When $N > 9$, the swamping event rate of the deletion-based greedy search algorithm increases sharply, and its post-positioning error becomes significantly larger than that of the proposed method.

B. Impacts of the Magnitude of Faults

In this section, we further study the impacts of fault magnitudes on the isolation and post-isolation positioning performance of the proposed method. A similar simulation procedure is conducted, but the variable of interest becomes the magnitude of faults. Using the geometry in Fig. 2, we randomly select nine satellites (measurements) for additional bias injection. Each bias is generated from a uniform distribution in the interval $[-M\ \text{m}, -\frac{M}{2}\ \text{m}] \cup [\frac{M}{2}\ \text{m}, M\ \text{m}]$. We study the cases of $M = \{5, 10, 20, 30, 40, 50, 65, 80, 100\}$, and for each case of M we conduct 10,000 simulations. The simulation parameters are listed in the "case B" row in Table IV.

Fig. 4 plots the simulation results. As can be seen, with the increase in fault magnitude, both methods show similar trends in the exactly correct detecting event rate. On the swamping event rate, the proposed method consistently maintains a small value, suggesting that the proposed method is less likely to exclude healthy measurements regardless of the fault magnitude. However, the greedy search method shows a large swamping rate in the cases of small-magnitude faults. With the increase in fault magnitude, the swamping rate of the greedy search method shows a decreasing trend. This could be explained by the mechanism of the deletion-based greedy search method that the increase in fault magnitude enlarges the difference between faulty and healthy measurements, thereby making it easier for the greedy search method to find the measurement that shows the most inconsistency with other measurements. Notably, the deletion-based greedy search method maintains zero masking event rate through all cases of fault magnitude. The proposed method has a large masking event rate when the injected faults have small magnitudes. Fig. 4(d) shows the change in the post-isolation positioning error of both methods. Although both methods show an increasing trend in the mean post-isolation positioning error, the magnitude of the positioning error remains within a small range, and the performance of both methods is comparable. It is interesting to find that the $99.5\,\%$ post-isolation positioning error of both methods shows a decreasing trend, which is opposite to the trend of their mean post-isolation positioning errors. This phenomenon actually indicates a trade-off between isolation performance and post-positioning performance in terms of fault magnitude. Although the increase in fault magnitude makes it easier to detect and isolate faults, an undetected fault with a large magnitude (which could occur because the exact correct detection rate is not 1) can cause greater damage to positioning accuracy; therefore, the mean post-isolation positioning errors would increase. On the contrary, small-magnitude faults are difficult to isolate but cause smaller impacts on positioning accuracy. Nevertheless, the events in which multiple faults are undetected are more frequent than the large magnitude situations. These events are occasional,

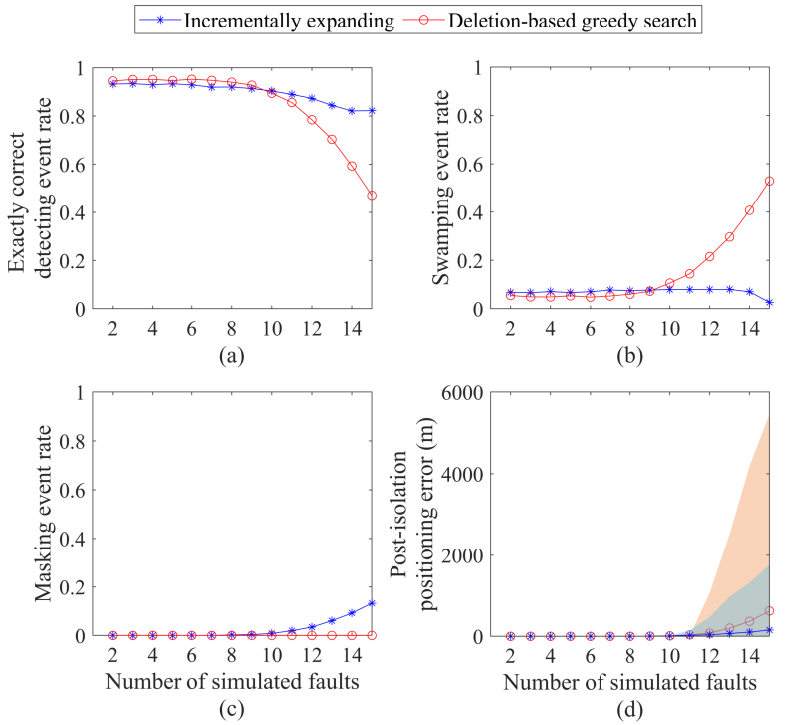

Fig. 3: The (a) exactly correct detecting event rate; (b) swamping event rate; (c) masking event rate; (d) mean post-isolation positioning error of two methods against the number of simulated faults with 3 constellations and fault magnitude uniformly distributed in $[-50\,\mathrm{m}, -25\,\mathrm{m}] \cup [25\,\mathrm{m}, 50\,\mathrm{m}]$. The blue and orange shaded areas in (d) are the $2.5\,\%$ $\sim$ $97.5\,\%$ percentile region of the post-isolation positioning error for the incrementally expanding and deletion-based greedy search methods, respectively.

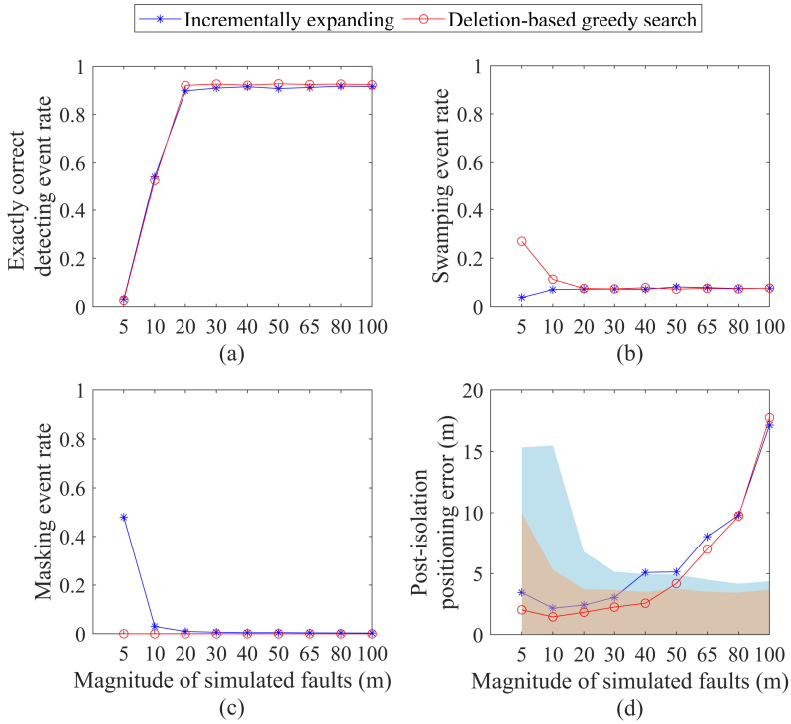

Fig. 4: The (a) exactly correct detecting event rate; (b) swamping event rate; (c) masking event rate; (d) mean post-isolation positioning error (the shaded area is bounded by the $2.5\,\%$ percentile and the $97.5\,\%$ percentile of the positioning error) of two methods against the magnitude of simulated faults with 3 constellations and 9 simultaneous faults. The blue and orange shaded areas in (d) are the $2.5\,\%$ $\sim$ $97.5\,\%$ percentile region of the post-isolation positioning error for the incrementally expanding and deletion-based greedy search methods, respectively.

and their impacts are reflected by the increase of the $99.5\,\%$ post-isolation positioning error, as shown in Fig. 4(d).

Given the results in Section V-A and Section V-B, the proposed algorithm shows a more stable performance in isolation and post-isolation positioning accuracy against the change in the number of faults and the fault magnitude when comparing to the deletion-based greedy search algorithm.

C. Analysis of Computation Complexity

This section analyzes and evaluates the time complexity of the proposed incrementally expanding algorithm. The proposed method consists of two algorithms, including the minimum basic set construction algorithm (Algorithm 1) and the incrementally expanding Algorithm for multiple faults isolation (Algorithm 2). In Algorithm 1, the "for" loop in lines 1–4 involves matrix operations, while lines 5–11 only consist of simple sorting operations (lines 5 and 9) and assignment operations (lines 6,7, and 10). Therefore, the main computation burden of Algorithm 1 is borne by the "for" loop in lines 1–4. The time complexity of Algorithm 1 can be regarded as $\mathcal{O}(n)$. Similar to Algorithm 1, the main computation burden of Algorithm 2 is born by matrix operations (lines 12 and 14). The other operations include simple sorting operations (line 18), assignment operations (lines 2, 4–6, 8–9, 16, 19, 21, and 30–31), and obtaining the inverse of standard distributions (lines 23 and 26). The "for" loop in lines 7–20 computes the studentized or Jackknife residual for each measurement and sorts these residuals in a grouping-based manner. In each group, the computation of residuals has a time complexity of $\mathcal{O}(\alpha_i n)$ (lines 10–17), where $\alpha_i < 1$. Therefore, the time complexity of the "for" loop in lines 7–20 is given by $\sum_i \mathcal{O}(\alpha_i n) = \mathcal{O}(n)$. Since the "while" loop in lines 3–32 has at most $n-m+1$ iterations, the worst-case time complexity of this "while" loop can be calculated by $\sum_{s=m+1}^{n-1} \mathcal{O}(n) = \mathcal{O}(n^2)$. Finally, the worst-case time complexity of Algorithm 2 is given by the summation of Algorithm 1 (line 1) and the "while" loop (lines 3–32), i.e., $\mathcal{O}(n) + \mathcal{O}(n^2) = \mathcal{O}(n^2)$.

Except for analyzing the worst-case time complexity, an additional analysis of the time complexity regarding the number of faults is conducted. Assuming that there are k faulty measurements and the proposed method can exactly isolate these faults, then the "while" loop in lines 3–32 of Algorithm 2 will have $n-m+1-k$ iterations. At this condition, the time complexity of this "while" loop is given by $\sum_{s=m+1}^{n-1-k} \mathcal{O}(n) = \mathcal{O}\left((n-k)n\right)$. Then, the time complexity of Algorithm 2 is given by $\mathcal{O}(n) + \mathcal{O}\left((n-k)n\right) = \mathcal{O}\left((n-k)n\right)$. Notably, this time complexity decreases with the increase of the number of faults k, which will be shown in the following experiments.

A Monte Carlo simulation is conducted to evaluate the computation time of the proposed method against the number of faults. To evaluate as many cases as possible, we adopt the geometry that contains the largest number of satellites in the worldwide simulation experiment, i.e., Fig. 2, for the experiment. Other configurations and the simulation procedure are the same as in Section V-A. For each number of faults, we conduct 10,000 simulations. All the computations are conducted using a laptop (Intel Core i7-12700H CPU, 2.30 GHz).

TABLE V: Computation time comparison in the three-constellation experiment

Number of faults	Proposed	Greedy search	Number of faults	Proposed	Greedy search
2	27.64 ms	1.94 ms	**9**	20.96 ms	6.65 ms
3	28.05 ms	2.73 ms	**10**	19.89 ms	7.28 ms
4	27.54 ms	3.49 ms	**11**	18.78 ms	8.02 ms
5	25.87 ms	4.10 ms	**12**	17.90 ms	8.62 ms
6	24.75 ms	4.78 ms	**13**	17.43 ms	9.37 ms
7	23.45 ms	5.41 ms	**14**	17.12 ms	10.40 ms
8	22.14 ms	6.02 ms	**15**	17.11 ms	11.26 ms

Table V compares the mean computation time of the proposed algorithm with the deletion-based greedy search algorithm for each number of faults. As can be seen, the mean computation time of the proposed algorithm is less than 30 ms for all cases, which is computationally efficient but slightly worse than the deletion-based greedy search algorithm. Moreover, the mean computation time of the proposed algorithm shows a decreasing trend with the increase in the number of faults, which reflects the expanding nature of the proposed algorithm. When the number of faults is large, the proposed methods require less expansion to find the cut-off point, as shown in (13). Therefore, the computation time is reduced with the increase in the number of faults. In contrast, the computation time of the deletion-based greedy search algorithm increases with the increase in the number of faults. This is because its time complexity is an increasing function of the number of faults, as illustrated in Appendix II.

VI. Application to Real-World Data with Artificially Injected Bias

A. Experiment Setting

This section examines the performance of the proposed method using reference station data from the Continuously Operating Reference Stations (CORS) website. Specifically, observation data from January 1st, 2023 are collected from the station CHTI at an interval of 30 seconds. Both single-frequency and dual-frequency (ionosphere-free combination) observations from three satellite constellations – GPS, Galileo, and GLONASS are considered. The position of the reference station is obtained from the RINEX file header, and the satellite position is calculated based on the broadcast ephemeris from NASA's Archive of Space Geodesy Data website [39] by utilizing RTKLIB [40]. The single-frequency pseudorange measurement is corrected by clock bias correction, ionospheric corrections, and tropospheric corrections based on RTKLIB [40] with the broadcast ephemeris [39], while the dual-frequency pseudorange measurement is corrected by clock bias correction and tropospheric corrections. Since the pseudorange data are retrieved every 30 seconds, we have 2,880 epochs in total. At each epoch, six measurements are randomly chosen for additional bias injection. Each bias is generated from a uniform distribution. The experiment setting is summarized in Table VI.

TABLE VI: Parameters of real-world data experiments with artificially injected bias

Case	Constellations	Number of faults	Fault magnitude	Alpha
Single-frequency	GPS, Galileo, GLONASS	6	$[-50\,\mathrm{m}, -25\,\mathrm{m}] \cup [25\,\mathrm{m}, 50\,\mathrm{m}]$	0.05
Dual-frequency	GPS, Galileo, GLONASS	6	$[-50\,\mathrm{m}, -25\,\mathrm{m}] \cup [25\,\mathrm{m}, 50\,\mathrm{m}]$	0.05

B. Performance Comparison

Table VII summarizes the rates of the three kinds of events in the case of single-frequency measurements. Similar to the worldwide simulation experiments, both methods have similar performance regarding the exact correct detecting event rate. The masking rate of the deletion-based greedy search method is nearly zero due to its deletion nature, which is remarkably smaller than that of the proposed method. However, the proposed method yields a significantly smaller swamping rate than that of the deletion-based greedy search method, achieving a $16.49\,\%$ reduction. Similar results are found in the results of the dual-frequency case, as shown in Table VIII. The swamping rate of the proposed method is $28.5\,\%$ smaller than that of the deletion-based greedy search method. However, the exactly correct detecting event rate of both methods is notably smaller than that in the single-frequency case. A possible reason is that the ionosphere-free combination of two frequency measurements increases the multipath and code noises at the receiver end. Since the model of the multipath and code noises is not $100\,\%$ accurate, the ionosphere-free combination enlarges the impacts of the inaccurate model of multipath and code noises on the estimation and fault isolation process, thereby reducing the exactly correct detecting event rate of both fault isolation methods.

TABLE VII: Isolation performance of real-data experiment with single-frequency measurements

Method	Exactly correct	Swamping	Masking
Incrementally expanding	$45.28\,\%$	**33.99** $\%$	$17.19\,\%$
Deletion-based greedy search	$49.06\,\%$	$50.48\,\%$	$0.03\,\%$

TABLE VIII: Isolation performance of real-data experiment with dual-frequency measurements

Method	Exactly correct	Swamping	Masking
Incrementally expanding	$2.89\,\%$	**62.14** $\%$	$20.21\,\%$
Deletion-based greedy search	$8.82\,\%$	$90.64\,\%$	$0.21\,\%$

Fig. 5(a) shows the cumulative distribution function (CDF) of the post-isolation positioning error of each method in the case of single-frequency measurements. As can be seen, the CDF curve of the proposed method is consistently above that of the deletion-based greedy search method, indicating that the proposed method has a higher probability of producing small post-isolation positioning errors than the deletion-based greedy search method. A similar trend is found in the dual-frequency case, as shown in Fig. 5(b). In statistics, the mean post-isolation positioning error of the proposed method is $31.97\,\mathrm{m}$, which is $15.5\,\%$ less than that of the deletion-based greedy search method ($37.84\,\mathrm{m}$) in the single-frequency case; the mean post-isolation positioning error of the proposed method is $57.1\,\mathrm{m}$, which is $14.8\,\%$ less than that of the deletion-based greedy search method ($67\,\mathrm{m}$). Again, the mean post-isolation positioning error of both methods is larger than that in the single-frequency case, which is potentially explained by the impacts of the enlarged multipath and code noises in the ionosphere-free combination.

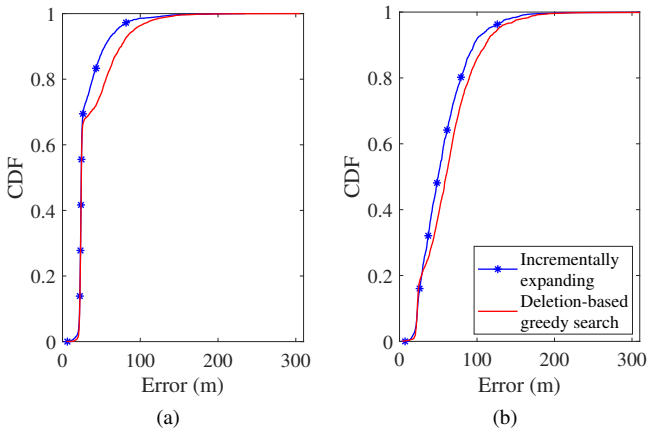

Fig. 5: CDF of the post-isolation positioning error of the two fault isolation methods in the (a) single-frequency and (b) dual-frequency cases.

VII. Conclusion and Future Work

This study proposes an expanding approach for detecting and isolating multiple faults in multi-constellation GNSS systems. The proposed method is designed to find the most consistent set by incrementally expanding the minimum basic set, which is constructed by the measurements with the smallest studentized residuals. In each expanding process, a grouping-based approach is developed to order measurements according to their studentized residuals and jackknife residuals. The heterogeneity of residuals associated with different constellations is considered in this approach. Subsequently, the no-fault hypothesis testing is conducted on the cut-off point of the expanded set. The expansion stops when a fault is detected.

The isolation performance of the proposed method and its impacts on positioning accuracy are examined in the worldwide simulations. Compared to the deletion-based greedy search method, the proposed method reduces the mean swamping event rate by more than $26\,\%$, suggesting that the proposed method is less likely to exclude healthy measurements. In addition, the mean post-isolation positioning error is reduced by $75\,\%$, which implies that the exclusion behavior of the proposed method causes less damage to the positioning system. The stability of the proposed method regarding the number of faults and fault magnitude is analyzed based on Monte Carlo simulations. Results show that the proposed method

has a more stable isolation and post-isolation positioning performance than the deletion-based greedy search method. Moreover, the computation load is comparable to the deletion-based greedy search method, suggesting its applicability in real-time positioning systems. An application to the real-world dataset with artificially injected bias is studied, where the proposed method yields a smaller swamping event rate and post-isolation positioning error than the deletion-based greedy-search method.

This study also has limitations, which also point out future research directions. As suggested by Table II, one of the main limitations of the proposed method is the high masking event rate when compared to the deletion-based greedy-search method. This value could be large when the number of faults increases or the faults have a small magnitude, as suggested by Fig. 3 and Fig. 4, respectively. In both cases, the minimum basic set is more likely to contain faulty measurements. Moreover, in the small-fault-magnitude case, it is difficult for the no-fault hypothesis testing to identify these faults, which slightly differ from healthy measurements. The key seems to be the construction of a fault-free minimum basic set. A possible solution could be integrating the deletion-based greedy search method that has excellent performance in the masking event rate into the construction of the minimum basic set, which will be the main focus of our future work.

APPENDIX I
STUDENTIZED AND JACKKNIFE RESIDUALS

Define $\tilde{\mathbf{y}}$, $\tilde{\mathbf{H}}$, and $\tilde{\boldsymbol{\varepsilon}}$ as follows:

$$\tilde{\mathbf{y}} = \boldsymbol{\Sigma}^{-\frac{1}{2}}\mathbf{y},\ \tilde{\mathbf{H}} = \boldsymbol{\Sigma}^{-\frac{1}{2}}\mathbf{H},\ \tilde{\boldsymbol{\varepsilon}} = \boldsymbol{\Sigma}^{-\frac{1}{2}}\boldsymbol{\varepsilon}\,, \tag{17}$$

where $\boldsymbol{\Sigma}^{-\frac{1}{2}}$ is the squared root of $\boldsymbol{\Sigma}^{-1}$, and is obtained by the Cholesky decomposition of $\boldsymbol{\Sigma}^{-1}$. The linearized pseudorange-based positioning System in (1) can be transferred to the following linear system:

$$\tilde{\mathbf{y}} = \tilde{\mathbf{H}}\Delta\mathbf{x} + \tilde{\boldsymbol{\varepsilon}}\,, \tag{18}$$

where $\tilde{\boldsymbol{\varepsilon}} \sim \mathcal{N}(0, \delta^2)$. The new system can be solved by the ordinary least square (OLS), and its solution is the same as that of (1). The studentized and jackknife residuals will be derived based on the new system.

A. Studentized Residual

Similar to the definition of the basic set in Section II-B, we define the basic set $\mathcal{B}$ (containing s measurements) in the new linear system and use the same symbol to simplify the notations. The measurement residual $\hat{\boldsymbol{\varepsilon}}_{\mathcal{B}}$ on $\mathcal{B}$ can be written as:

$$\hat{\boldsymbol{\varepsilon}}_{\mathcal{B}} = \tilde{\mathbf{y}}_{\mathcal{B}} - \tilde{\mathbf{H}}_{\mathcal{B}}\Delta\hat{\mathbf{x}} = (\mathbf{I} - \tilde{\mathbf{G}}_{\mathcal{B}})\tilde{\mathbf{y}}_{\mathcal{B}}\,, \tag{19}$$

where

$$\tilde{\mathbf{G}}_{\mathcal{B}} = \tilde{\mathbf{H}}_{\mathcal{B}}(\tilde{\mathbf{H}}_{\mathcal{B}}^T\tilde{\mathbf{H}}_{\mathcal{B}})^{-1}\tilde{\mathbf{H}}_{\mathcal{B}}^T \tag{20}$$

is the projection matrix. Then $\hat{\boldsymbol{\varepsilon}}_{\mathcal{B}}$ has a multi-variate Gaussian distribution $\mathcal{N}(0, (\mathbf{I} - \tilde{\mathbf{G}}_{\mathcal{B}})\delta^2)$. For the ith measurement in the full set and belongs to $\mathcal{B}$, its residual $\hat{\varepsilon}_i$ has a marginal Gaussian distribution $\mathcal{N}(0, (1-\tilde{g}_{\mathcal{I}_{\mathcal{B}}(i)})\delta^2)$, where $\tilde{g}_{\mathcal{I}_{\mathcal{B}}(i)}$ is the $\mathcal{I}_{\mathcal{B}}(i)$th element on the diagonal of $\tilde{\mathbf{G}}_{\mathcal{B}}$, and $\mathcal{I}_{\mathcal{B}}(\cdot)$ is a function to identify the index of y_i in $\mathcal{B}$. The studentized residual of $y_i \in \mathcal{B}$ is defined by

$$r_i = \frac{\hat{\varepsilon}_i}{\delta\sqrt{1 - \tilde{g}_{\mathcal{I}_{\mathcal{B}}(i)}}}\,. \tag{21}$$

Note that δ is assumed to be unknown. To obtain an estimate for δ, the sum of square error (SSE) on $\mathcal{B}$ is calculated as follows:

$$\text{SSE} = \hat{\boldsymbol{\varepsilon}}_{\mathcal{B}}^T\hat{\boldsymbol{\varepsilon}}_{\mathcal{B}} = \tilde{\mathbf{y}}_{\mathcal{B}}^T(\mathbf{I} - \tilde{\mathbf{G}}_{\mathcal{B}})\tilde{\mathbf{y}}_{\mathcal{B}}\,. \tag{22}$$

The expectation of SSE is given by

$$\begin{aligned} &E[\text{SSE}] \\ =&\text{trace}\Big[(\mathbf{I} - \tilde{\mathbf{G}}_{\mathcal{B}})\text{Cov}[\tilde{\mathbf{y}}_{\mathcal{B}}]\Big] + E[\tilde{\mathbf{y}}_{\mathcal{B}}]^T(\mathbf{I} - \tilde{\mathbf{G}}_{\mathcal{B}})E[\tilde{\mathbf{y}}_{\mathcal{B}}] \\ =&\text{trace}\Big[(\mathbf{I} - \tilde{\mathbf{G}}_{\mathcal{B}})\delta^2\mathbf{I}\Big] + (\tilde{\mathbf{G}}_{\mathcal{B}}\Delta\hat{\mathbf{x}})^T(\mathbf{I} - \tilde{\mathbf{G}}_{\mathcal{B}})(\tilde{\mathbf{G}}_{\mathcal{B}}\Delta\hat{\mathbf{x}})\,. \end{aligned} \tag{23}$$

Since $\tilde{\mathbf{G}}_{\mathcal{B}}\Delta\hat{\mathbf{x}}$ belongs to the space spanned by the columns of $\tilde{\mathbf{G}}_{\mathcal{B}}$ and this space is orthogonal to the space spanned by the columns of $\mathbf{I} - \tilde{\mathbf{G}}_{\mathcal{B}}$, we have

$$(\mathbf{I} - \tilde{\mathbf{G}}_{\mathcal{B}})(\tilde{\mathbf{G}}_{\mathcal{B}}\Delta\hat{\mathbf{x}}) = 0\,. \tag{24}$$

Therefore,

$$E[\text{SSE}] = \text{trace}\Big[(\mathbf{I} - \tilde{\mathbf{G}}_{\mathcal{B}})\delta^2\mathbf{I}\Big] = \delta^2\sum_k^n \lambda_k\,, \tag{25}$$

where $\lambda_k, k \in 1, 2, \cdots, s$ are the eigenvalues of $\mathbf{I} - \tilde{\mathbf{G}}_{\mathcal{B}}$. It is known that $\mathbf{I} - \tilde{\mathbf{G}}_{\mathcal{B}}$ has $s - m$ eigenvalues taking 1 and m eigenvalues taking 0. Therefore,

$$E[\text{SSE}] = (s - m)\delta^2\,, \tag{26}$$

and $\sqrt{\frac{\text{SSE}}{s-m}}$ is the unbiased estimator of δ.

Replace δ in (21) with $\sqrt{\frac{\text{SSE}}{s-m}}$, and then the studentized residual can be written by

$$r_i = \frac{\hat{\varepsilon}_i}{\sqrt{\frac{\text{SSE}}{s-m}}\sqrt{1 - \tilde{g}_{\mathcal{I}_{\mathcal{B}}(i)}}} = \frac{\tilde{y}_i - \tilde{\mathbf{h}}_{\mathcal{I}_{\mathcal{B}}(i)}\Delta\hat{\mathbf{x}}}{\sqrt{\frac{\hat{\boldsymbol{\varepsilon}}_{\mathcal{B}}^T\hat{\boldsymbol{\varepsilon}}_{\mathcal{B}}}{s-m}}\sqrt{1 - \tilde{g}_{\mathcal{I}_{\mathcal{B}}(i)}}}\,, \tag{27}$$

where $\tilde{\mathbf{h}}_{\mathcal{I}_{\mathcal{B}}(i)}$ is the $\mathcal{I}_{\mathcal{B}}(i)$th row of $\tilde{\mathbf{H}}_{\mathcal{B}}$. Finally, variables in the original linear system in (1) can be recovered by doing the inverse operation in (17) as follows:

$$r_i = \frac{\sqrt{w_{\mathcal{I}_{\mathcal{B}}(i)}}y_i - \sqrt{w_{\mathcal{I}_{\mathcal{B}}(i)}}\mathbf{h}_{\mathcal{I}_{\mathcal{B}}(i)}\Delta\hat{\mathbf{x}}_{\mathcal{B}}}{\sqrt{\frac{\left(\mathbf{y}_{\mathcal{B}} - \mathbf{H}_{\mathcal{B}}\Delta\hat{\mathbf{x}}_{\mathcal{B}}\right)^T\mathbf{W}_{\mathcal{B}}\left(\mathbf{y}_{\mathcal{B}} - \mathbf{H}_{\mathcal{B}}\Delta\hat{\mathbf{x}}_{\mathcal{B}}\right)}{s-m}}\sqrt{1 - g_{\mathcal{I}_{\mathcal{B}}(i)}}}\,, \tag{28}$$

where $w_{\mathcal{I}_{\mathcal{B}}(i)}$ is the $\mathcal{I}_{\mathcal{B}}(i)$th element on the diagonal of $\mathbf{W}_{\mathcal{B}} = \boldsymbol{\Sigma}_{\mathcal{B}}^{-1}$, $\mathbf{h}_{\mathcal{I}_{\mathcal{B}}(i)}$ is the $\mathcal{I}_{\mathcal{B}}(i)$th row of $\mathbf{H}_{\mathcal{B}}$, and $g_{\mathcal{I}_{\mathcal{B}}(i)}$ is the $\mathcal{I}_{\mathcal{B}}(i)$th element on the diagonal of $\mathbf{G}_{\mathcal{B}}$ defined in (4). This ends the proof of (5).

B. Jackknife Residual

For each measurement $\tilde{y}_i$ in the non-basic set $\mathcal{O}$, the difference between the predicted measurement and $\tilde{y}_i$ is given by

$$\begin{aligned} \tilde{\epsilon}_i =& \tilde{\mathbf{h}}_i\Delta\hat{\mathbf{x}}_{\mathcal{B}} - \tilde{y}_i \\ =& \tilde{\mathbf{h}}_i\Delta\hat{\mathbf{x}}_{\mathcal{B}} - (\tilde{\mathbf{h}}_i\Delta\mathbf{x}_{\mathcal{B}} + \tilde{\varepsilon}_i)\,, \end{aligned} \tag{29}$$

where $\tilde{\mathbf{h}}_i$ is re-constructed based on the OLS solution on $\mathcal{B}$. The reconstruction process is similar to that in the original linear system, as shown in (9). Since $\tilde{\varepsilon} \sim \mathcal{N}(0, \delta^2)$, $\Delta\hat{\mathbf{x}}_{\mathcal{B}}$ is the unbiased estimator of $\Delta\mathbf{x}$ and has a Gaussian distribution. The variance of $\Delta\hat{\mathbf{x}}_{\mathcal{B}}$ can be calculated by

$$\begin{aligned}\mathrm{Var}[\Delta\hat{\mathbf{x}}_{\mathcal{B}}] &= \left(\tilde{\mathbf{H}}_{\mathcal{B}}^T\tilde{\mathbf{H}}_{\mathcal{B}}\right)^{-1}\tilde{\mathbf{H}}_{\mathcal{B}}^T\mathrm{Var}[\tilde{\mathbf{y}}_{\mathcal{B}}]\tilde{\mathbf{H}}_{\mathcal{B}}\left(\tilde{\mathbf{H}}_{\mathcal{B}}^T\tilde{\mathbf{H}}_{\mathcal{B}}\right)^{-1} \\ &= \left(\tilde{\mathbf{H}}_{\mathcal{B}}^T\tilde{\mathbf{H}}_{\mathcal{B}}\right)^{-1}\tilde{\mathbf{H}}_{\mathcal{B}}^T\mathrm{Var}[\tilde{\varepsilon}_{\mathcal{B}}]\tilde{\mathbf{H}}_{\mathcal{B}}\left(\tilde{\mathbf{H}}_{\mathcal{B}}^T\tilde{\mathbf{H}}_{\mathcal{B}}\right)^{-1} \\ &= \left(\tilde{\mathbf{H}}_{\mathcal{B}}^T\tilde{\mathbf{H}}_{\mathcal{B}}\right)^{-1}\delta^2\,.\end{aligned} \tag{30}$$

$\tilde{\varepsilon}_i$ also has a Gaussian distribution $\mathcal{N}(0, \delta^2)$. Therefore, $\tilde{\epsilon}_i$ is Gaussian distributed, and its mean can be calculated by

$$E[\tilde{\epsilon}_i] = \tilde{\mathbf{h}}_i E[\Delta\hat{\mathbf{x}}_{\mathcal{B}} - \Delta\mathbf{x}_{\mathcal{B}}] - E[\tilde{\varepsilon}_i] = 0\,, \tag{31}$$

and its variance can be calculated by

$$\begin{aligned}\mathrm{Var}[\tilde{\epsilon}_i] &= \tilde{\mathbf{h}}_i\mathrm{Var}[\Delta\hat{\mathbf{x}}_{\mathcal{B}}]\tilde{\mathbf{h}}_i^T + \mathrm{Var}[\tilde{\varepsilon}_i] \\ &= \tilde{\mathbf{h}}_i\left(\tilde{\mathbf{H}}_{\mathcal{B}}^T\tilde{\mathbf{H}}_{\mathcal{B}}\right)^{-1}\tilde{\mathbf{h}}_i^T\delta^2 + \delta^2\,.\end{aligned} \tag{32}$$

Then the jackknife residual is defined as the normalized $\tilde{\epsilon}_i$ as follows:

$$\tilde{t}_i = \frac{\tilde{\epsilon}_i}{\delta\sqrt{\tilde{\mathbf{h}}_i\left(\tilde{\mathbf{H}}_{\mathcal{B}}^T\tilde{\mathbf{H}}_{\mathcal{B}}\right)^{-1}\tilde{\mathbf{h}}_i^T + 1}}\,. \tag{33}$$

By replacing δ in (33) with $\sqrt{\frac{\mathrm{SSE}}{s-m}}$ and recovering the variables in the original linear system in (1), the jackknife residual can be written as

$$\begin{aligned}\tilde{t}_i &= \frac{\sqrt{w_i}y_i - \sqrt{w_i}\mathbf{h}_i\Delta\hat{\mathbf{x}}_{\mathcal{B}}}{\hat{\delta}\sqrt{1 + w_i\mathbf{h}_i\left(\mathbf{H}_{\mathcal{B}}^T\mathbf{W}_{\mathcal{B}}\mathbf{H}_{\mathcal{B}}\right)^{-1}\mathbf{h}_i^T}} \\ \hat{\delta} &= \sqrt{\frac{\left(\mathbf{y}_{\mathcal{B}} - \mathbf{H}_{\mathcal{B}}\Delta\hat{\mathbf{x}}_{\mathcal{B}}\right)^T\mathbf{W}_{\mathcal{B}}\left(\mathbf{y}_{\mathcal{B}} - \mathbf{H}_{\mathcal{B}}\Delta\hat{\mathbf{x}}_{\mathcal{B}}\right)}{s-m}}\,,\end{aligned} \tag{34}$$

where $\mathbf{h}_i$ is defined in (9). This ends the proof of (8).

Appendix II
Deletion-based Greedy Search Algorithm

The deletion-based greedy-search algorithm removes the measurement with the largest normalized residual at each step [21]. Specifically, define Ξ_k as the measurement set at time step k, and then the positioning solution with Ξ_k is given by (utilizing WLS in an iterative approach)

$$\Delta\hat{\mathbf{x}}_{\Xi_k} = \left(\mathbf{H}_{\Xi_k}^T\mathbf{W}_{\Xi_k}\mathbf{H}_{\Xi_k}\right)^{-1}\mathbf{H}_{\Xi_k}^T\mathbf{W}_{\Xi_k}\mathbf{y}_{\Xi_k} \tag{35a}$$

$$\hat{\mathbf{x}}_{\Xi_k} = \mathbf{x}_0 + \Delta\hat{\mathbf{x}}_{\Xi_k}\,, \tag{35b}$$

where $\mathbf{W}_{\Xi_k} = \mathbf{\Sigma}_{\Xi_k}^{-1}$ is the weighting matrix. The subscript Ξ_k in (35) indicates that the corresponding variable is defined with respect to the set Ξ_k. The weighted sum of square error (WSSE) is given by

$$\mathrm{WSSE} = \left(\mathbf{y}_{\Xi_k} - \mathbf{H}_{\Xi_k}\Delta\hat{\mathbf{x}}_{\Xi_k}\right)^T\mathbf{W}_{\Xi_k}\left(\mathbf{y}_{\Xi_k} - \mathbf{H}_{\Xi_k}\Delta\hat{\mathbf{x}}_{\Xi_k}\right). \tag{36}$$

With the Gaussian assumption $\boldsymbol{\varepsilon} \sim \mathcal{N}(0, \delta^2\mathbf{\Sigma})$ in Section II-A and the fault-free assumption about Ξ_k, WSSE has a chi-squared distribution with the degrees of freedom (DOF) of $n_k - m$, where n_k is the size fo Ξ_k and m is the number of unknown variables to be solved. If

$$\mathrm{WSSE} > \chi^{2^{-1}}_{n_k-m}(\alpha)\,, \tag{37}$$

potential faults exist in Ξ_k, where α is the false alarm rate. Then, for each measurement y_i in Ξ_k, the normalized residual is given by:

$$r_i = \frac{w_i(y_i - \mathbf{h}_i\Delta\hat{\mathbf{x}}_{\Xi_k})^2}{1 - w_i\mathbf{h}_i\left(\mathbf{H}_{\Xi_k}^T\mathbf{W}_{\Xi_k}\mathbf{H}_{\Xi_k}\right)^{-1}\mathbf{h}_i^T}\,, \tag{38}$$

where w_i is the ith element on the diagonal of $\mathbf{W}_{\Xi_k}$, y_i is the ith element of $\mathbf{y}_{\Xi_k}$, and $\mathbf{h}_i$ is the ith row of $\mathbf{H}_{\Xi_k}$. A time complexity of $\mathcal{O}(n-s+1)$ is associated with this operation, where $s = 1, 2, \cdots, n-(m+1)$ is the numbering of the current step. Then, the algorithm removes the measurement with the largest r_i. The above process repeats until WSSE is lower than the threshold, where a consistent set is found, or until the number of remaining measurements is no larger than $m+1$. Therefore, the worst-case time complexity of the deletion-based greedy search algorithm is given by $\sum_{s=1}^{n-(m+1)}\mathcal{O}(n-s+1) \approx \mathcal{O}(n^2)$. Assuming that there are $k < n$ faulty measurements and the deletion-based greedy search algorithm can exactly isolate these faults, then this algorithm will have k iterations. The time complexity of the deletion-based greedy search algorithm is now given by $\sum_{s=1}^{k}\mathcal{O}(n-s+1) \approx \mathcal{O}(kn)$, which increases with the increase of the number of faults k.

Appendix III
More Results

This section shows the result of worldwide simulations with the four-constellation setting, as listed in Table IX. Specifically, Table X summarizes the rate of the three kinds of events in this simulation, Fig. 6 compares the map of post-isolation positioning errors for both methods, and Table XI shows the statistics of the post-isolation positioning error of all location-time combinations of both methods. Similar conclusions can be drawn as those in Section IV.

TABLE IX: Parameters of worldwide simulations with four constellations

Constellations	Number of faults	Fault magnitude	Alpha
GPS, Galileo, GLONASS, BEIDOU	12	$[-50\,\mathrm{m}, -25\,\mathrm{m}]\cup[25\,\mathrm{m}, 50\,\mathrm{m}]$	0.05

TABLE X: Isolation performance in four-constellation experiment

	Incrementally expanding			Deletion-based greedy search		
Event	Exact	Swamping	Masking	Exact	Swamping	Masking
Max	**93.06** %	**16.67** %	12.15 %	88.54 %	54.51 %	**0** %
Mean	**84.86** %	**10.09** %	4.09 %	68.66 %	31.31 %	**0** %
Min	**72.92** %	**5.56** %	0 %	45.49 %	11.46 %	**0** %

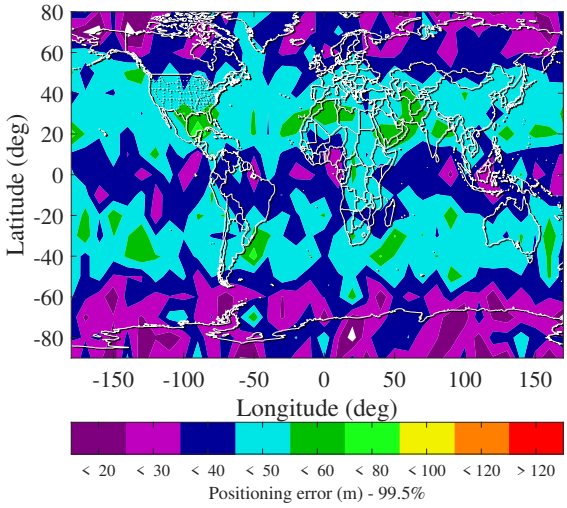

(a)

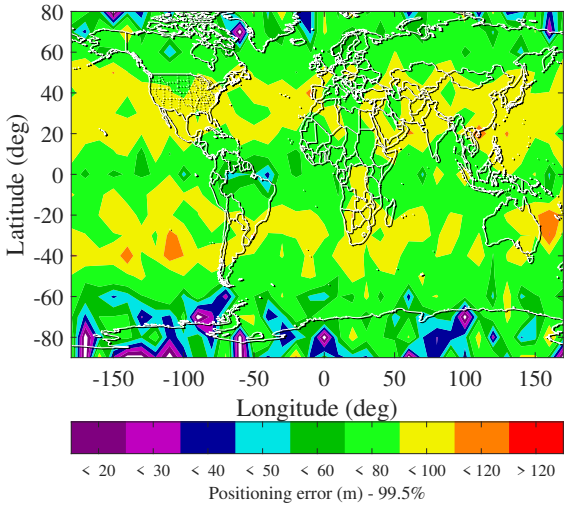

(b)

Fig. 6: 99.5 percentile of the post-isolation positioning error over the course of the day yielded by (a) the incrementally expanding algorithm and (b) the deletion-based greedy search algorithm in the worldwide simulation experiment with four constellations.

TABLE XI: Statistics of the post-isolation positioning error for all location-time combinations in the four-constellation experiment

Incrementally expanding			Deletion-based greedy search		
Max	Mean	Min	Max	Mean	Min
89.80 m	**1.99** m	0.01 m	176.33 m	4.04 m	0.01 m

REFERENCES

[1] Y. Fang, H. Min, W. Wang, Z. Xu, and X. Zhao, "A fault detection and diagnosis system for autonomous vehicles based on hybrid approaches," *IEEE Sensors Journal*, vol. 20, no. 16, pp. 9359–9371, 2020.

[2] O. Osechas, P. Misra, and J. Rife, "Carrier-phase acceleration RAIM for GNSS satellite clock fault detection," *NAVIGATION*, vol. 59, no. 3, pp. 221–235, 2012.

[3] X. Han, Y. Hu, A. Xie, X. Yan, X. Wang, C. Pei, and D. Zhang, "Quadratic-kalman-filter-based sensor fault detection approach for unmanned aerial vehicles," *IEEE Sensors Journal*, vol. 22, no. 19, pp. 18 669–18 683, 2022.

[4] M. Joerger and B. Pervan, "Fault detection and exclusion using solution separation and Chi-squared ARAIM," *IEEE Transactions on Aerospace and Electronic Systems*, vol. 52, no. 2, pp. 726–742, 2016.

[5] Y. Liu and Y. J. Morton, "Improved automatic detection of GPS satellite oscillator anomaly using a machine learning algorithm," *NAVIGATION*, vol. 69, no. 1, 2022.

[6] Z. Gao, S. X. Ding, and C. Cecati, "Real-time fault diagnosis and fault-tolerant control," *IEEE Transactions on Industrial Electronics*, vol. 62, no. 6, pp. 3752–3756, 2015.

[7] G. Betta and A. Pietrosanto, "Instrument fault detection and isolation: State of the art and new research trends," *IEEE Transactions on Instrumentation and Measurement*, vol. 49, no. 1, pp. 100–107, 2000.

[8] R. G. Brown, "A baseline GPS RAIM scheme and a note on the equivalence of three RAIM methods," *Navig. J. Inst. Navig.*, vol. 39, no. 3, pp. 301–316, 1992.

[9] FAA, "Phase II of the GNSS evolutionary architecture study," Federal Aviation Administration, Tech. Rep., 2010.

[10] H. Chen, R. Sun, Q. Cheng, and L. Yang, "A factor set-based gnss fault detection and exclusion for vehicle navigation in urban environments," *GPS Solutions*, vol. 27, no. 2, p. 87, 2023.

[11] M. Joerger and B. Pervan, "Kalman filter-based integrity monitoring against sensor faults," *Journal of Guidance, Control, and Dynamics*, vol. 36, no. 2, pp. 349–361, Mar. 2013. [Online]. Available: https://arc.aiaa.org/doi/10.2514/1.59480

[12] Y. C. Lee, "Analysis of range and position comparison methods as a means to provide GPS integrity in the user receiver," in *Proceedings of the 42nd Annual Meeting of The Institute of Navigation (1986)*, 1986, pp. 1–4.

[13] B. W. Parkinson and P. Axelrad, "Autonomous GPS integrity monitoring using the pseudorange residual," *NAVIGATION*, vol. 35, no. 2, pp. 255–274, 1988.

[14] M. A. Sturza, "Navigation system integrity monitoring using redundant measurements," *NAVIGATION*, vol. 35, no. 4, pp. 483–501, 1988.

[15] B. S. Pervan, D. G. Lawrence, C. E. Cohen, and B. W. Parkinson, "Parity space methods for autonomous fault detection and exclusion using GPS carrier phase," in *Proceedings of Position, Location and Navigation Symposium-PLANS'96*. IEEE, 1996, pp. 649–656.

[16] B. S. Pervan, S. P. Pullen, and J. R. Christie, "A multiple hypothesis approach to satellite navigation integrity," *NAVIGATION*, vol. 45, no. 1, pp. 61–71, 1998.

[17] T. Walter and P. Enge, "Weighted RAIM for precision approach," in *Proceedings of the 8th International Technical Meeting of the Satellite Division of The Institute of Navigation (ION GPS 1995)*, 1995, pp. 1995–2004.

[18] S. Hutsell, M. Forsyth, and C. B. McFarland, "One-way GPS time transfer: 2002 performance," in *Proceedings of the 34th Annual Precise Time and Time Interval Systems and Applications Meeting*, 2002, pp. 69–76.

[19] J. Blanch, T. Walker, P. Enge, Y. Lee, B. Pervan, M. Rippl, A. Spletter, and V. Kropp, "Baseline advanced RAIM user algorithm and possible improvements," *IEEE Transactions on Aerospace and Electronic Systems*, vol. 51, no. 1, pp. 713–732, 2015.

[20] L. Carlone, A. Censi, and F. Dellaert, "Selecting good measurements via ℓ_1 relaxation: A convex approach for robust estimation over graphs," in *2014 IEEE/RSJ International Conference on Intelligent Robots and Systems*. IEEE, 2014, pp. 2667–2674.

[21] J. Blanch, T. Walker, and P. Enge, "Fast multiple fault exclusion with a large number of measurements," in *Proceedings of the 2015 International Technical Meeting of The Institute of Navigation*, 2015, pp. 696–701.

[22] D. Knowles and G. Gao, "Detection and exclusion of multiple faults using Euclidean distance matrices," in *Proceedings of the 36th International Technical Meeting of the Satellite Division of The Institute of Navigation (ION GNSS+ 2023)*, 2023, pp. 1774–1782.

[23] C. Zhu, M. Meurer, and M. Joerger, "Integrity analysis for greedy search based fault exclusion with a large number of faults," in *2023 IEEE/ION Position, Location and Navigation Symposium (PLANS)*. IEEE, 2023, pp. 430–435.

[24] L.-T. Hsu, "Analysis and modeling GPS NLOS effect in highly urbanized area," *GPS Solutions*, vol. 22, no. 1, p. 7, 2018.

[25] Y.-E. Lee, A.-L. Tao, and S.-S. Jan, "Combined algorithm for satellite selection for open-sky and constrained environments," in *Proceedings of the 30th International Technical Meeting of the Satellite Division of the Institute of Navigation (ION GNSS+ 2017)*, 2017, pp. 3680–3693.

[26] L. T. Hsu, H. Tokura, N. Kubo, Y. Gu, and S. Kamijo, "Multiple faulty GNSS measurement exclusion based on consistency check in urban canyons," *IEEE Sensors Journal*, vol. 17, no. 6, pp. 1909–1917, 2017.
[27] F. Kianifard and W. H. Swallow, "Using recursive residuals, calculated on adaptively-ordered observations, to identify outliers in linear regression," *Biometrics*, pp. 571–585, 1989.
[28] V. Barnett and T. Lewis, *Outliers in Statistical Data*. Wiley New York, 1994, vol. 3, no. 1.
[29] A. S. Hadi and J. S. Simonoff, "Procedures for the identification of multiple outliers in linear models," *Journal of the American statistical association*, vol. 88, no. 424, pp. 1264–1272, 1993.
[30] A. Atkinson and H.-M. Mulira, "The stalactite plot for the detection of multivariate outliers," *Statistics and Computing*, vol. 3, pp. 27–35, 1993.
[31] C. Bonferroni, "Teoria statistica delle classi e calcolo delle probabilita," *Pubblicazioni del R Istituto Superiore di Scienze Economiche e Commericiali di Firenze*, vol. 8, pp. 3–62, 1936.
[32] A. J. Pope, "The Statistics of Residuals and the Detection of Outliers," NOAA Technical Report, Rockville, Tech. Rep., 1976.
[33] J. W. Tukey, "Bias and confidence in not quite large samples," *Annals of Mathematical Statistics*, vol. 29, p. 614, 1958.
[34] M. H. Quenouille, "Notes on bias in estimation," *Biometrika*, vol. 43, no. 3/4, pp. 353–360, 1956.
[35] A. C. Aitken, "On least squares and linear combination of observations," *Proceedings of the Royal Society of Edinburgh*, vol. 55, pp. 42–48, 1936.
[36] S.-S. Jan, W. Chan, T. Walter, and P. Enge, "Matlab simulation toolset for SBAS availability analysis," in *Proceedings of the 14th International Technical Meeting of the Satellite Division of The Institute of Navigation (ION GPS 2001)*, 2001, pp. 2366–2375.
[37] J. Blanch, T. Walter, and P. Enge, "RAIM with optimal integrity and continuity allocations under multiple failures," *IEEE Transactions on Aerospace and Electronic Systems*, vol. 46, no. 3, pp. 1235–1247, 2010.
[38] Y. Zheng, F. Zheng, C. Yang, G. Nie, and S. Li, "Analyses of glonass and gps+ glonass precise positioning performance in different latitude regions," *Remote Sensing*, vol. 14, no. 18, p. 4640, 2022.
[39] NASA. Broadcast ephemeris data. [Online]. Available: https://cddis.nasa.gov/Data_and_Derived_Products/GNSS/broadcast_ephemeris_data.html
[40] T. Takasu and A. Yasuda, "Development of the low-cost RTK-GPS receiver with an open source program package RTKLIB," in *International symposium on GPS/GNSS*, vol. 1. International Convention Center Jeju Korea Seogwipo-si, Republic of Korea, 2009, pp. 1–6.

Penggao Yan received the bachelor's degree in Communication Engineering in 2018 and the master's degree in Pattern Recognition and Intelligent Systems in 2021, both from Wuhan University, China. He is currently a Ph.D. Candidate at the Department of Aeronautical and Aviation Engineering, Faculty of Engineering, Hong Kong Polytechnic University.

His research interests include non-Gaussian noise modeling, fault detection and integrity monitoring in localization systems, and control-aided localization.

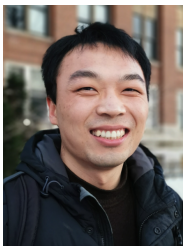

Yingjie Hu received the bachelor's degree in automotive engineering in 2017 from Tongji University and master's degree in aerospace engineering in 2022 from University of Minnesota, Twin Cities. He is currently pursuing his Ph.D. degree in Aerospace Engineering in University of Minnesota, Twin Cities.

His research interests include: State estimation, Sensor fusion, Integrity and Overbounding.

Welson Wen (Member, IEEE) received a BEng degree in Mechanical Engineering from Beijing Information Science and Technology University (BISTU), Beijing, China, in 2015, and an MEng degree in Mechanical Engineering from the China Agricultural University, in 2017. After that, he received a Ph.D. degree in mechanical engineering, the Hong Kong Polytechnic University. He was a visiting student researcher at the University of California, Berkeley (UCB) in 2018. He is currently an assistant professor in the Department of Aeronautical and Aviation Engineering, the Hong Kong Polytechnic University.

His research interests include multi-sensor integrated localization for autonomous vehicles, SLAM, and GNSS positioning in urban canyons.

Li-Ta Hsu (Senior Member, IEEE) received the B.S. and Ph.D. degrees in aeronautics and astronautics from National Cheng Kung University, Taiwan, in 2007 and 2013, respectively. He is currently an associate professor at the Department of Aeronautical and Aviation Engineering, Faculty of Engineering, Hong Kong Polytechnic University, before he served as a post-doctoral researcher in Institute of Industrial Science at University of Tokyo, Japan. In 2012, he was a visiting scholar in University College London, U.K. He is an Associate Fellow of RIN.

His research interests include GNSS positioning in challenging environments and localization for pedestrians, autonomous driving vehicles, and unmanned aerial vehicles.